Aerosol growth in CO_2 absorption with MEA, modelling and comparison with experimental results

H.F. Svendsen [a,*], H. Majeed [a], H.K. Knuutila [a], M. Hillestad [a], S. Evjen [b], T. Mejdell [c], A. Einbu [c], K.W. Hjarbo [c], G. Haugen [c], K.A. Hoff [c]

[a] *Department of Chemical Engineering, NTNU, 7491 Trondheim Norway*
[b] *Department of Chemistry, NTNU, 7491 Trondheim Norway*
[c] *Sintef Industry, NO-7465 Trondheim, Norway*

ARTICLE INFO

ABSTRACT

A new and improved aerosol model has been developed and tested against experimental data. An e-NRTL equilibrium model for MEA was extended to cover sulphuric acid containing droplets and validated against new eboulliometer data in this work.

The droplet model predicts emissions without demister installed in the absorber, within $\pm$ 20% and with demister, 30-80% of the measured emissions. The model predicts well the change in emissions from NG-based to coal-based exhaust.

Under conditions reported in this work, the droplet number concentration was found to have a small effect on predicted emissions because of more MEA gas-phase depletion with high droplet concentrations and slower growth. The effects counteract each other. With significant MEA depletion in the gas phase, the emissions are largely determined by the mass transfer rate from the bulk liquid.

The initial droplet sulphuric acid concentration had a minor effect on the outlet droplet size distribution. The effect on MEA emissions was significant: the emissions went up with increased initial sulphuric acid concentration. The effect of sulphuric acid was stronger for low inlet gas CO_2 concentration (NG) than for coal-based exhaust. The increase in emissions is believed to be caused by the increase in overall driving force for MEA between bulk liquid phase and droplets.

The log-normal model does not catch small inlet droplet sizes in the range below 20-30nm. These droplet sizes hardly grow in the absorber and water wash and in the total emissions, these droplets have a negligible impact on emissions.

1. Introduction

During the last decade, the problem of aerosol formation and growth in amine-based post-combustion CO_2 capture plants has received much interest and research due to the high amine emissions that can be encountered, (Knudsen et al. (2011), Kamijo et al. (2013), da Silva et al. (2013), Mertens et al. (2012, 2013), Carter (2012), Bade et al. (2014), Lombardo et al. (2017), Fujita et al. (2017) and Mejdell et al. (2021)). Several experimental studies have been performed to investigate the performance of various measurement techniques for aerosol number concentration and size distribution such as Phase Doppler Interferometry (PDI), Condensation Particle Counter(CPC) and Electric Low Pressure Impactor(ELPI+), and to use them for aerosol characterization (Brachert et al. (2014), Khakharia et al. (2013, 2015, 2016), Mertens et al. (2012, 2014a, 2014b), Fulk and Rochelle (2014, 2017), Beaudry et al. (2017)). These works discuss and compare the methods and their limitations.

In parallel to the experimental studies, models for droplet growth and composition have been developed. Fulk and Rochelle (2013) started with the gas phase profile from an Aspen Plus simulation and assumed a droplet moving with the gas in the absorber. To predict droplet growth, mass and energy balances for the drop were formulated and in the mass transfer, partial pressure effects caused by curvature, the Kelvin effect, and the Knudsen correction for small size were considered (Fuchs and Sutugin (1971), Davis(1982) and Qu and Davis (2001)). Khakharia et al. (2014) also used Aspen Plus and implemented a stage-wise procedure where the mass and heat balances between gas and bulk liquid were solved first, then mass and heat transfer to the droplets was taken into

account. No details regarding mass and heat transfer models are given, but the model resulted in outlet emissions predictions. Kang et al. (2017) improved the model by Fulk and Rochelle (2013) and included gas phase depletion of the amine and showed how the droplet growth was affected by droplet number concentration. Zhang et al. (2017) used the model to predict aerosol growth at realistic plant conditions. Majeed et al. (2017a, 2017b) and Majeed and Svendsen (2018a, 2018b) developed a two-dimensional model, accounting for droplet internal profiles and the partial pressure and mass transfer corrections mentioned earlier: The Kelvin and Knudsen effects. As a basis, bulk liquid phase profiles for composition and temperature from the CO2SIM process simulator were used, see (Einbu (2016))

Development in droplet growth and composition in the absorber and water wash sections was shown, and the effect of variation in inlet gas composition on emissions discussed. Also, the effect of changing parameters such as lean amine temperature and height of water wash column and temperatures was shown. Kang et al. (2020) developed a multi-scale model using Aspen Plus simulations for the absorber and gPROMS for the droplets, including the Kelvin and Knudsen corrections. They performed experiments using a droplet generator for a sucrose solution and could compare modelling results with experiments. All the mentioned models rely on droplets entering the absorber with a single size. Majeed et al. (2018c) improved the single droplet size model to consider a droplet size distribution based on a log-normal distribution function.

In the present work we have further improved the droplet distribution model. It has become more robust and the equilibrium model for MEA has been expanded to cover droplets containing H_2SO_4. Ebulliometer measurements on mixtures of MEA and H_2SO_4 were performed for six compositions and five temperatures and used in developing the MEA/ H_2SO_4 model. SO_3 in the gas phase will, upon supersaturation, form H_2SO_4 containing droplets which will absorb MEA that is neutralized by the acid. This can affect growth and composition development.

Predictions from the model are compared with experimental results from pilot plant tests at the Tiller CO_2 facility in Trondheim. Droplets containing H_2SO_4 were generated using a Topas droplet generator and the inlet droplet size distribution was measured using ELPI+. Two independent instruments, ELPI+ and PDI, were used to measure the outlet distribution. Finally, droplet number counts were made by ELPI+ and CPC and FTIR monitored the emissions from the plant. Gas compositions mimicking both NG and coal-based exhaust were used.

2. Models

2.1. The MEA/H_2SO_4/water model

The aerosol droplet growth and amine emissions model discussed in earlier papers (Majeed et al., 2017a, b, 2018c; Majeed and Svendsen, 2018a, b does not deal with sulphuric acid droplets. The model assumes either pure water or 5M MEA droplets entering the absorber with different initial sizes. Characterization of aerosol emissions from CO_2 capture plants will not be complete without considering the possibility of SO_3 or sulfuric acid droplets. To consider the effect of sulphuric acid, a new MEA/water/CO_2/sulfuric acid equilibrium model, based on an earlier MEA e-NRTL model, see Putta et al. (2016), was developed where H_2SO_4 was added and the pertinent chemical and VLE equilibrium constants refitted to new ebulliometer data and data for the water/-H_2SO_4 system up to 60 wt% H_2SO_4 (Perry and Green (2007)). This model was used for the whole range of compositions from pure water, mixtures of water and H_2SO_4 and for the CO_2/MEA/water/ H_2SO_4 blends. In the acidic range, the vapor pressure of MEA was assumed negligible.

The droplet viscosity affects the internal diffusivities of CO_2 and MEA. The viscosity model used is according to (Hartono et al. (2014)) and considers both amine concentration and loading. The relationship

between viscosity and diffusivity is modelled according to (Snijder et al. (1993)).

2.2. Demister model

A model for the demister used in the pilot plant was implemented in the aerosol model. The demister is modelled, using a generalized approach according to (AMACS (2004), Anonymous (2005), Bürkholz (1989)). The efficiency curve: Figure 5 in (AMACS (2004)), was functionalized and used to calculate the separation efficiency of the various droplet sizes. The only parameters in the model that can be changed are the demister specific surface area and the wire diameter. The demister used in the experiments was a Becoil (Begg-Cousland) H type with a nominal specific surface area of $360 m^2/m^3$ and wire diameter 0.28mm.

2.3. Growth model

As mentioned in the introduction, the model used in this work is a modification of the model presented in (Majeed et al. (2018c)). This model was based on volume growth and had some stability issues for small droplets (<20 nm). In this work the model is based on growth in droplet radius.

The model for a single droplet, as given in Majeed et al. (2018c), is:

$$\frac{dV}{dt} = \frac{N_{total} \cdot A}{\rho_{droplet}} = \widetilde{N} \cdot A$$

Here N_{total} is the mass flux into the droplet, A is the droplet surface area, V the droplet volume, $\rho_{droplet}$ droplet density and t time.

By introducing the equation for the volume of a sphere, the equation reduces to:

$$\frac{dR}{dt} = \frac{N_{total}}{\rho_{droplet}} = \widetilde{N}$$

The droplet model describes how the distribution will change with time or position. The model includes mass and energy transfer over the droplet surface and reactions within the droplet. Note that the volumetric flux $\widetilde{N}$ is the rate at which the radius increases or decreases with time. Here we assume that droplets do not break or aggregate.

With a large population of droplets, the population distribution function f can be approximated by a continuous function of the size R. The population distribution function f will change with time and is, therefore, a function f(t;R). We require that the integral of the population distribution overall sizes is unity at any time.

$$\int_0^\infty f(t,R)dR = 1$$

The population distribution may be approximated by two parameters, the number average radius $\overline{R_1} = \langle R \rangle$ and the size average radius $\overline{R_2} = \langle R^2 \rangle / \langle R \rangle$ as (Ashgriz, 2011; Biesenberger and Sebastian, 1983):

$$\overline{R_1} = \int_0^\infty Rf(t,R)dR = \langle R \rangle \tag{3}$$

$$\overline{R_2} = \frac{\int_0^\infty R^2 f(t,R)dR}{\int_0^\infty Rf(t,R)dR} = \frac{\langle R^2 \rangle}{\langle R \rangle} \tag{4}$$

The ratio between these two parameters, $\overline{R_1}$ and $\overline{R_2}$, describes the width of the distribution. The larger the ratio, the wider the distribution. It is obvious that $\overline{R_2} > \overline{R_1}$. We cannot describe all possible distribution by two parameters, but unimodal distributions are quite accurately described.

These two parameters are useful because the ratio between them is a measure of the distribution variance or dispersion of sizes. The radius variance is defined as:

$$\sigma_V^2 = \int_0^\infty f(t,R)\left(R - \overline{R_1}\right)^2 dR = \langle R^2 \rangle - \overline{R_1}^2$$

And the ratio is therefore:

$$\frac{\overline{R_2}}{\overline{R_1}} = 1 + \left(\frac{\sigma_V}{\overline{R_1}}\right)^2$$

The change in radius average with respect to time is equal to the time derivative of the number average radius:

$$\frac{d\overline{R_1}}{dt} = \left\langle \frac{dR}{dt} \right\rangle = \left\langle \tilde{N}_1 \right\rangle = \tilde{N}_1 \tag{5}$$

It is here assumed that the mass flux into all $\overline{R_1}$ droplets is the same.

The time derivative of the size average radius, i.e. how it is changing with respect to time, can be written as;

$$\frac{1}{\overline{R_2}}\frac{d\overline{R_2}}{dt} = \frac{1}{\langle R^2 \rangle}\frac{d\langle R^2 \rangle}{dt} - \frac{1}{\overline{R_1}}\frac{d\overline{R_1}}{dt} \tag{6}$$

The time derivative of the average square radius is;

$$\frac{d\langle R^2 \rangle}{dt} = 2\left\langle R\frac{dR}{dt} \right\rangle = 2\left\langle R\tilde{N}_2 \right\rangle \tag{7}$$

Now, by inserting Eqs. 5 and 7 in Eq. 6, the final derivative of the size average volume with respect to time will take the form;

$$\frac{d\overline{R_2}}{dt} = \frac{2}{\overline{R_1}}\left\langle R\tilde{N}_2 \right\rangle - \frac{\overline{R_2}}{\overline{R_1}}\left\langle \tilde{N}_1 \right\rangle = \frac{2}{\overline{R_1}}\tilde{N}_2\langle R\rangle - \frac{\overline{R_2}}{\overline{R_1}}\tilde{N}_1 \tag{8}$$

In order to implement this model, we need to assume a probability density function f. As in Majeed et al. (2018c), since R > 0, a log normal distribution is used to approximate the size distribution of the aerosols as (Johnson et al., 1994);

$$f(R) = \frac{1}{R\sigma\sqrt{2\pi}}exp\left(-\frac{(\ln R - \mu)^2}{2\sigma^2}\right) \tag{9}$$

Where R is the radius limit over which the function is integrated, σ is the variance and μ indicates the mean. The variance and mean are;

$$\sigma = \sqrt{\ln \frac{\overline{R_2}}{\overline{R_1}}}$$

$$\mu = \ln \overline{R_1} - \frac{1}{2}\ln \frac{\overline{R_2}}{\overline{R_1}}$$

3. Experimental

3.1. Ebulliometer

The aerosol droplet growth and amine emissions model discussed in earlier papers (Majeed et al., 2017a, b, 2018c; Majeed and Svendsen, 2018a, b) does not deal with sulphuric acid droplets. It only discusses either pure water or 5M MEA droplets entering the absorber with different initial sizes. Characterization of aerosol emissions from CO_2 capture plants will not be complete without considering the possibility of SO_3 or sulfuric acid droplets. To consider the effect of sulphuric acid, a new NRTL model, with species comprising MEA; CO_2, H_2O and H_2SO_4, was developed as already explained in an earlier section.

Therefore, ebulliometer experiments were performed for the unloaded water/MEA/H_2SO_4 system. Six different water/MEA/H_2SO_4 concentrations were tested, four in the acidic range and two with excess MEA. The experiments were performed at five temperatures giving in total 30 data points. In the tests with excess sulphuric acid, only the total pressure was measured, and it was assumed that this was equal to the water vapour pressure.

The ebulliometer techniques used were the same as in our previous work (Hartono et al. (2013), Kim et al. (2008) and Trollebø et al. (2020)

and are not repeated here. The concentration of MEA in the liquid and withdrawn gas samples was analysed by IC. The vapour phase MEA analyses have an accuracy of $\pm10\%$ because of the low concentrations.

3.2. Pilot plant

The testing was done using a 15m absorber column receiving flue gas from a propane burner. The absorber and water wash system, including Topas droplet generator, direct contact cooler, measurement sections and the layout of the gas flow path, is given in the Appendix, Figure A1. The absorption column has a 20 cm inner diameter and is equipped with 15-meter structured packing (Mellapak 2X) divided into three sections. Liquid distributor and redistributor sections (in-house design) are installed between each section. The maximum solvent flow rate is 16-22 l/min depending on the viscosity of the liquid and the pressure in the desorber. The column is well-instrumented with temperature sensors every meter and pressure sensors below each packed column section and above the upper water wash section. Each of the sections is designed for representative sampling of gas and liquid. One measurement section is placed just before the absorber inlet and here ELPI+, CPC and PDI measurements were performed. After leaving the upper column packing section, another measuring section for aerosols is installed. Here, ELPI+, CPC and PDI measurements were also performed. A demister (Becoil H, Begg Cousland) is fitted above the lean solvent distributor and before the measuring section. From the absorber, the gas flows upwards and is redirected 180° before it is piped downwards and into the water wash section. The water-wash section, with 2.4 m height of structured Mellapak 2X packing, is used to remove amine vapour in the flue gas. During the last part of the campaign, the demister was removed and replaced with a special Bluefil demister, and a final experiment series was run without demister.

As mentioned above, a propane burner was used to generate flue gas. The CO_2-content in the flue gas entering the pre-treatment conditioning column (DCC) can be adjusted by either diluting the exhaust gas with fresh air or by adding CO_2 re-cycled from the top of the stripper. The DCC is a direct contact cooler/conditioner to obtain a well-defined humidity and temperature of the feed gas into the absorber. The DCC is a column with 2.5 m height with a Mellapak 2X structured packing (inner diameter 26 cm). Aerosols from the Topas atomizer aerosol generator were introduced into the warm (50-56 °C for NG and 83°C for coal exhaust) unsaturated flue gas before it was cooled and water-saturated in the DCC. A high capacity fan (500 m3 /h) was positioned downstream the DCC. Before entering the absorber, the gas flows through a measuring section designed for aerosol measurement equipment.

The solvent loading was determined by analysing the amine and CO_2 concentrations in the solvent using acid-base titration and TIC/TOC analyser (operated in TIC mode).

3.3. Measurements

Phase Doppler Interferometry (PDI) measures the particle size distribution, total particulate concentration, and velocity of an aerosol cloud, as described by Bachalo (1980). The analyser used in this work is a custom-made instrument designed and built by Artium Technologies Inc. (California, USA). The instrument is built to measure aerosol drops between 0.3 and 12.0 µm in diameter at aerosol concentrations greater than 100/cm [3]. The PDI instrument is based on in-situ measurement in a 1" diameter channel. The physical layout of the optics of the PDI instrument did not allow for positioning of the instrument measurement cell directly into the gas duct of the pilot plant. Thus, a dedicated duct section was built to obtain a representative gas sample flow in a bypass duct tailored to accommodate the PDI. These sampling sections were located in the gas duct of the absorber gas intake, in the measurement section on top of the absorption column and on top of the water wash section of the plant. A controllable fan and a gas rotameter were placed downstream the PDI in order to enable isokinetic sampling in the duct to

Table 1
Pilot plant operating conditions

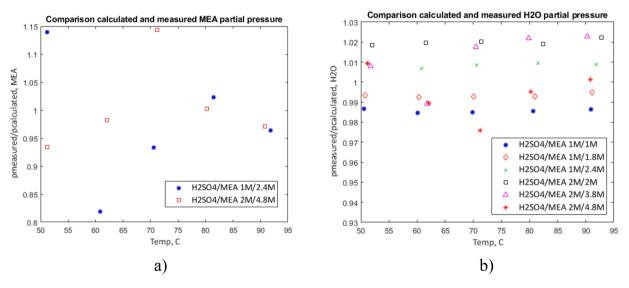| RUN	Gas flow m³/hour	Inlet CO₂ vol% dry	Outlet CO₂ vol% dry	Lean loading mole CO₂ /mole amine	Rich loading mole CO₂ /mole amine	Gas inlet temperature, °C	Lean amine temperature, °C	Aerosol measurements
3	250	4.57	0.93	0.17	0.47	35	NA	CPC – in abs PDI – out abs ELPI+ - in abs FTIR – out WW
4	250	4.56	0.91	0.16	0.46	35	NA	CPC – in abs PDI – out abs ELPI+ - out abs FTIR – out WW
14	160	13.0	2.38	0.17	0.47	35	39.4	CPC – in abs PDI – out abs FTIR – out WW
15	250	4.35	0.96	0.16	0.45	35	42.5	CPC – in abs PDI – out abs FTIR – out WW
20	250	4.35	1.18	0.16	0.45	35	41	CPC – out abs PDI – out abs FTIR – out WW

Figure 1. Ratio of experimental over predicted vapour pressure of a) MEA and b) Water as function of composition and temperature.

the PDI. he PDI measurements reported in this work were conducted as measurement performed over time periods of varying duration at stable plant conditions. Sampling duration of 300 seconds was aimed for, but not always achieved by the instrument during dense mist conditions due to limitations in the data collection buffer capacity. Typical sampling criteria invoked a counts threshold of around 10 000 counts or a sampling time of 5 minutes.

A **Condensation Particle Counter (CPC)** can measure the total particle concentration of ultrafine and nanoparticles suspended in air or other carrier gases. The CPC instrument applied in this work was a UF-CPC 200 from Palas. The instrument is capable of measuring particle number densities up to $2 \bullet 10^6$ particles/cm³ in single count mode and 10^7 particles/cm³ in nephelometric (photometric) mode without diluting of the sampled gas. Only single count mode was applied for the reported CPC measurements in this work. The CPC measurements were performed at the sampling points in the same measurement sections as the PDI sampling to achieve measurements of the same aerosol sample.

The **Electrostatic Low-Pressure Impactor (ELPI+),** produced by by DEKATI™, is a real-time particle spectrometer that provides the total particle number concentration and the particle size distribution (PSD) of aerosols/particulate matter (PM) present in a gas stream. The measurement range is between 0.009 and 10 μm. Particles larger than 10 μm are impacted on a cut-off stage and are not measured. The instrument

gives results in uncorrected and corrected form, the latter considering that droplets below about 20nm may not be counted properly. Previous studies revealed that dilution and heating may have an effect on the measured particle size distribution. In particular, shrinking is observed in the presence of high H_2SO_4 concentrations due to the evaporation of water from the aerosols (Brachert et al. (2014), Mertens et al. (2014), Saha and Irwin (2017)). For RUN 3 and RUN4 (see Table 1) of the tests, the particles in the flue gas were characterized at the absorber inlet at the absorber outlet respectively by Engie Laborelec to evaluate the aerosols growth inside the absorber column.

The **ATM 241 Topas droplet generator** was supplied by Topas GmbH generating distributions of droplets from a desired solution. It has four nozzles and can operate with up to 2.2 bar. In this work the droplets were generated with the following settings: 4 nozzles, 1.6 bar and 0.2 wt % H_2SO_4 as solution.

The gaseous MEA emissions were monitored continuously with **Fourier Transform Infrared Spectroscopy (FTIR)**. The FTIR, allowing online measurement of the emissions, was located after the water wash section. FTIR does not differentiate between the aerosol and volatile amine emissions, and it was used to measure the overall solvent emissions. Manual sampling was also done and comparisons with the FTIR results agreed very well.
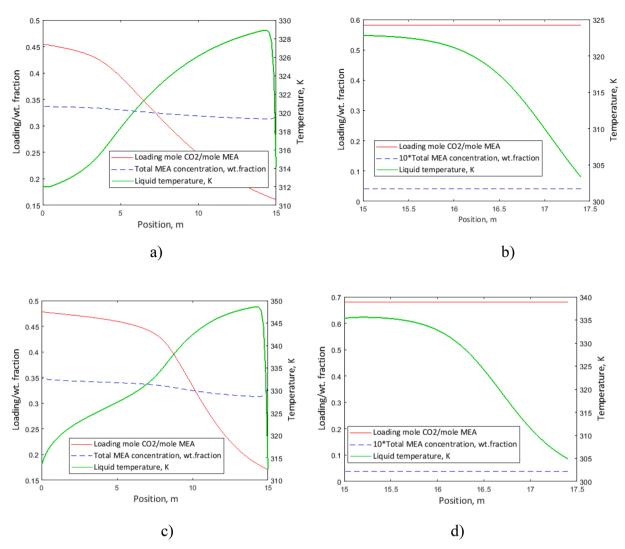
Figure 2. Liquid phase concentration and temperature profiles from CO2SIM simulation. a) Run 15 and 20, inlet CO_2 content 4.35 %(dry), absorber, b) Run 15 and 20, inlet CO_2 content 4.35 %(dry), water wash c) Run 14, inlet CO_2 content 13.0 %(dry), absorber, d) Run 14, inlet CO_2 content 13.0 %(dry), water wash

3.4. The modelled pilot runs

Five experimental runs are used in this work for comparison with model predictions. In Table 1 are given the main operating conditions for the runs used. RUN 3 concentrated on measuring the inlet size distribution, using ELPI+. RUN 4 was a replica of RUN 3, focusing on the outlet measurements using ELPI+, CPC, and FTIR. RUN 14 was for coal-based exhaust. RUN 15, which was a close replica of RUN 4, is used in the comparisons. RUN 20 was a replica of RUN 15 but without demister installed.

Run 14 mimicked a coal flue gas case with an inlet CO_2 content of 13 vol% on a dry basis, whereas the other runs simulated a natural gas case with an inlet CO_2 content of 4.35-4.56 vol% on dry basis. Run 14 was run with a superficial gas velocity of 1.42 m/s and Run 4, 15 and 20 with 2.21 m/s.

4. Results

4.1. NRTL model with species comprising MEA, CO2, H2O and H2SO4

Ebulliometer experiments were performed for the unloaded water/MEA/H_2SO_4 system covering different water/MEA/H_2SO_4 concentrations in both the acidic and excess MEA- range. The resulting data are given in Table A1 in the appendix, and Figure 1 shows a comparison

between model predictions and obtained experimental data.

We see that the scatter for MEA (Figure 1a), is much larger than for water, but apart from three points, the deviations between model and experiments are below 10%. The main uncertainty in the MEA data is the vapour phase analyses, which in these tests were done by IC. For water, the deviations are mostly below 2% (Figure 1b). In total, this is deemed satisfactory considering the experimental uncertainty in the vapour pressure measurements for MEA. The measured MEA vapour pressures are from 30-70% of the vapour pressures predicted by the MEA model without H_2SO_4 and the water vapour pressures are lowered by about 10-15%. As we do not have measurements for CO_2-loaded solutions, it is assumed that the CO_2 equilibrium remains unchanged.

In order to verify that the MEA and MEA/H_2SO_4 models behave similarly at zero acid concentration, we tested the two eNRTL models against each other. The concentration of H_2SO_4 was set to zero in the model containing H_2SO_4 in the test. In this validation the initial droplet size distribution was defined with diameters 161 and 1017 nm, respectively, in line with the measured corrected distribution. No change in outlet distribution was found.

4.2. Modelling of pilot runs from the Tiller campaign

ELPI+ was used to measure absorber inlet distribution in Run 3 and the droplet size distributions at the absorber outlet in Run 4 as
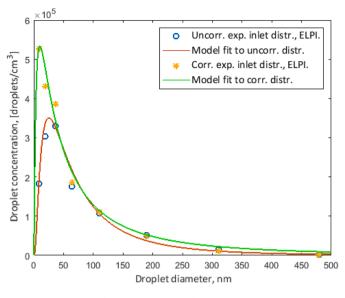
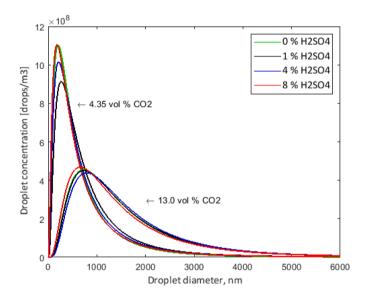**Figure 3.** Inlet droplet size distribution for Tiller RUN 3

Figure 4. The effect of inlet sulphuric acid concentration

mentioned earlier. Run 3 and Run 4 had identical operating conditions. The inlet droplet size distribution based on ELPI+ from Run 3 was used as basis for all droplet size simulations as the droplet generator settings were the same.

The process simulator (CO2SIM) was used to obtain the absorber and water wash bulk liquid phase composition and temperature profiles, see Figure 2. The simulations used the experimental lean loadings, flue gas compositions and temperatures as well as lean solvent temperature as starting points. The rich loading and CO_2 capture rate were predicted well by the model with 0.47 mole CO_2/mole MEA and 2.3vol% for RUN 14 and 0.45 mole CO_2/mole MEA and 1.08 vol% for RUN 15 and RUN 20, close to the experimental values given in Table 1. For the Tiller Runs 14, 15 and 20, the profiles are given below and used as a basis for the aerosol model. Profiles for RUN 3 and 4 are not given as the operating conditions were almost identical to RUN 15.

4.3. Inlet droplet distribution

The inlet droplet size distribution to the absorber for RUN 3 was measured by ENGIE Laborelec using the ELPI+. This instrument

measures down to very small droplet sizes but was found unable to register sizes above approximately 300-500nm. The inlet size distribution is a function of the operating conditions in the Topas droplet generator, i.e. the number of nozzles used, the initial H_2SO_4 concentration and the pressure. It was assumed that the droplet production and size distribution from the Topas would be the same when using the same settings, regardless of the exhaust gas composition and flowrate.

In Figure 3 are given two experimental inlet distributions. For the points denoted "Uncorr." all the data from the ELPI+ measurements were used as produced by the instrument. For the points denoted "Corr.", a correction was employed to counteract the effect of partial missing detection of the smallest droplet sizes below 20nm. The two distributions were both fitted to a log-normal distribution function and Figure 3 shows that the fits are reasonably good. The fit to the uncorrected ELPI+ data gave characterizing diameters of 101 and 256nm for the log-normal distribution, whereas the corrected data gave 161 and 1017nm for the two diameters. These results are used in the further modelling.

The total number of droplets counted by ELPI+ for the used Topas settings was 1.16-1.17e6 droplets/cm^3 for the uncorrected count and 1.7e6 droplets/cm^3 for the corrected count. The CPC measured about 960000 droplets/cm^3. We have used both the ELPI+ counts in the subsequent absorber modelling.

4.4. The effect of sulfuric acid content

The inlet droplet swarm was generated by the Topas droplet generator which was filled with 0.2 wt % aqueous sulphuric acid. After the TOPAS, the generated droplets enter the exhaust gas pipe. The exhaust gas had a temperature of 50-83°C and almost all the water evaporates. Modelling tests performed showed that nearly all water would disappear after less than 0.5s and the retention time in the pipe was 3-5s. The exhaust gas stream with particles is then passed on to the direct contact cooler, (DCC), where water will condense on the droplets and make them grow before entering the absorber. The inlet droplet size distribution measurements were done just before the absorber. The sulphuric acid concentration at this point was not measured and not exactly known. In order to study the effect of this uncertainty, the aerosol model was run with 4 different sulphuric acid concentrations, 0, 1, 4 and 8 wt %. All were run with the corrected inlet droplet size distribution. The results are shown in Figure 4.

We see that the outlet droplet size increases with increasing sulphuric acid concentration. This is reasonable because of two effects. The sulphuric acid containing droplets have lower water vapour pressure than pure water. This results in less water evaporation when the droplets enter the absorber, and they actually shrink less at the absorber inlet than without sulphuric acid. Also, MEA will rapidly transfer to the droplets and react with the sulphuric acid. This will give very low MEA vapour pressure above the droplet surface as long as free sulphuric acid exists. Thus, MEA mass transfer will be rapid. When the sulphuric acid is neutralized, MEA and CO_2 will transfer to the droplets almost as if the sulphuric acid was not there. The only effect will be the change in activity coefficients. We see that the effect of sulphuric acid on outlet droplet size distribution is apparently rather weak. The reason for this is that in the final droplets, the amount of sulphuric acid is very small, and the final droplet growth is therefore not affected to any considerable extent. In this work we have used 4% H_2SO_4 in the inlet droplets as standard.

4.5. Droplet growth and profiles, RUN 14 and 15

The CO2SIM profiles for RUN 14 and 15 are shown in Figure 2. RUN 15 is a natural gas exhaust case with CO_2 content 4.35% and RUN 14 is a coal-based exhaust case with CO_2 content 13%. Details are given in Table 1. As seen, for both cases the CO2SIM simulation predicts high loadings in the water washes and an increase in temperature from the absorber top to the water wash bottom. All profiles further shown are
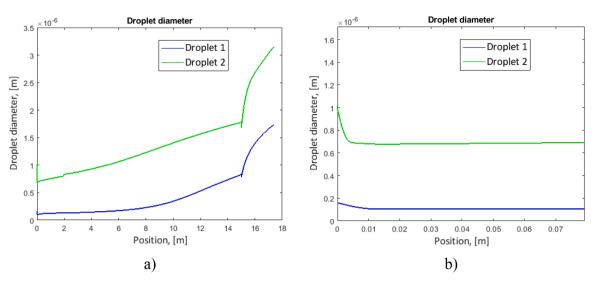
Figure 5. Droplet diameter as a function of position in absorber and water wash, RUN 15, Natural gas exhaust. a) whole column, b) magnified inlet section. In the figure the initial droplet sizes are: Droplet 1 = 161 nm and Droplet 2 = 1017 nm.

based on the corrected inlet droplet distribution (161 and 1017 nm) and using a demister specific area of 50 m^2/m^3 unless otherwise noted.

In Figure 5 for RUN 15, we see the predicted droplet diameter profiles. The profiles for RUN 14 are similar and not shown here. With a sulfuric acid content of 4 wt%, the droplets initially shrink because of water evaporation. This is also observed without sulphuric acid, but then the effect is much stronger (Majeed and Svendsen 2018a and Majeed, et al. 2017b). The main reasons for this are the low water content in the inlet gas, and the sharp temperature increase as the gas with droplets enter the absorber. So, even though the droplet sulphuric acid content will reduce the water vapour pressure compared to pure water, the temperature increase still gives a driving force from the droplets to the gas. The droplets' response is much faster than the response from the bulk liquid, the latter which will increase the gas water vapour pressure. Thus, the sulphuric acid concentration in the droplets builds up to about 2.8 mole/L as seen in Figure 8. MEA absorbs rapidly, as seen in Figure 6, and the sulphuric acid is neutralized. Also, CO$_2$ is absorbed extremely fast, as seen in Figure 7. All this lowers the water vapour pressure; water starts condensing and the droplets begin to grow. The diameter of the largest droplet decreases initially much more than for the small droplet. This is reasonable as it takes more MEA to neutralize the sulphuric acid in the larger droplet, about 250 times as much, and the surface is only 40 times larger. After the initial stage, the droplets grow continuously through the absorber. After the demister, located between the absorber and water wash section, the largest droplets are removed, and the two defining diameters are reduced before they increase again in the water wash section.

Figure 6 a) and b) shows the MEA profiles through the absorber and water wash. We see that the concentration of protonated MEA rises sharply at the inlet, showing the neutralization of sulphuric acid. As the droplets grow, the concentration of sulphuric acid decreases, shown in Figure 8, the carbamate concentration increases and becomes about the same as the concentration of protonated MEA as the sulphuric acid concentration becomes insignificant. As expected, the free MEA concentration increases through the absorber as the loading goes down. In the water wash, the loading is high, and the free MEA concentration is very low. The total MEA concentration is also reduced significantly. The jumps seen about 1 m into the absorber are located where the sulfuric acid is fully neutralized by MEA. The total MEA concentration reaches the bulk liquid amine concentration after about 5m. This is in line with earlier findings, see (Majeed and Svendsen (2018a)). It should be remembered that the droplets grow, increasing the amount of MEA needed to reach the bulk liquid concentration. The water vapor pressure

above the droplets quickly reaches close to equilibrium with the gas phase water vapor pressure as shown in Figure 6 C.

Figure 7 shows the concentration profiles for bound CO$_2$, as carbamate, and free CO$_2$. Initially, the free CO$_2$ concentration rises very sharply, much faster than the concentration of carbamate. Carbamate is produced in competition with the neutralization of sulfuric acid. MEA must diffuse into the droplet, neutralize H$_2$SO$_4$, and simultaneously partly react with CO$_2$. The formation of carbamate only really picks up after all sulphuric acid is neutralized. After the initial stage, the carbamate concentrations start rising, and as expected, more rapidly in the small droplet than in the large one.

The sulphuric acid concentration profiles are shown in Figure 8. Figure 8 b) shows the profiles for the bottom part of the absorber. We see that the sulphuric acid concentration increases sharply because of the decreasing size of the droplets. The maximum in concentration coincides with the minimum in size. As MEA diffuses into the droplets, H$_2$SO$_4$ is converted to HSO$_4^-$ and SO$_4^{2-}$. Because of the high viscosity of the droplets and subsequent low diffusivity, all the sulphuric acid is neutralized and converted to SO$_4^-$ only after about 2m. The neutralization is faster in the small droplet (large droplet not shown), but the increase in sulphuric acid concentration is about the same in both droplets. The drop in sulfuric acid concentration at about 1 m coincides with a similar drop for MEA and happens when all H$_2$SO$_4$ is neutralized. This is probably an artifact caused by the equilibrium model for the water vapour pressure. This artifact was checked, and it has an insignificant impact on the final result.

Figure 9 a) shows the temperature profiles through absorber and water wash. The droplet and gas-phase temperatures follow the liquid phase profile closely apart from when changes become very fast, as at the absorber bottom and at the lean amine inlet. The liquid exiting the water wash has a higher temperature than the top absorber temperature and droplets and gas are heated up when entering the water wash. The CO$_2$ partial pressure profile in Figure 9 b) shows that the final CO$_2$ partial pressure is 0.9 kPa and very close to the experimental value.

The MEA partial pressure profile is shown in Figure 10. The gas-phase depletion is seen to be important as the gas phase partial pressure is much lower than the saturation pressure above the absorber's bulk liquid. We see that the droplets are in close equilibrium with the bulk gas phase and, if no aerosol is removed, the emissions will be determined to a large extent by the amine mass transfer from the bulk liquid phase. A similar behaviour was observed in the models of (Zhang et al. (2017))

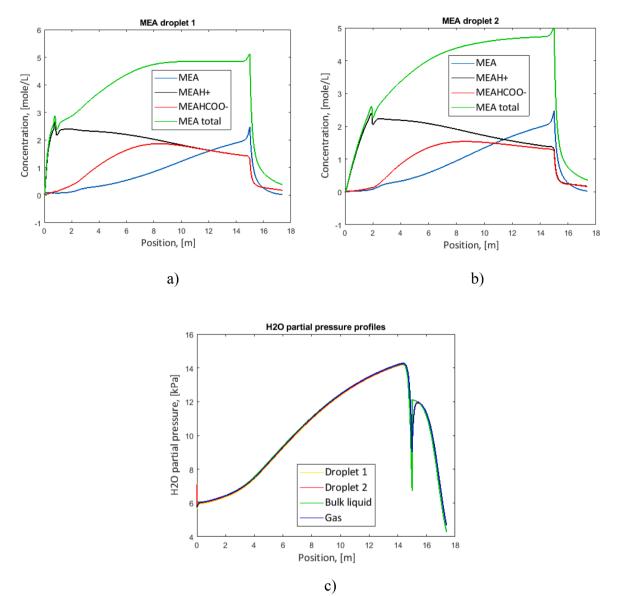In the water wash the MEA concentration falls rapidly, partly caused

a)

b)

c)

Figure 6. a) and b) RUN 15, natural gas exhaust. MEA component concentrations as a function of position in absorber and water wash. c) Water partial pressure over the droplets. In the figure the initial droplet sizes are: Droplet 1 = 161 nm and Droplet 2 = 1017 nm.

by desorption since the bulk phase MEA partial pressure is very low because of low MEA concentration and high CO_2 loading, and partly because of fast growth in droplets size. We see that the driving forces for MEA are very low and slightly lower for the small droplet compared with the large droplet. This is caused by the small size of droplets and thereby high surface to volume ratio.

Figure 11 shows the droplet size distributions at the water wash inlet with and without demister. Also, the model fit to the distribution after the demister is given. We see that without demister, the model maps the distribution perfectly. This was expected since the log-normal distribution is kept throughout the absorber and since no droplets are removed in the demister, the distribution is still log-normal. With a demister, as shown in Figure 11A, droplets are removed according to size and the resulting distribution will not be log-normal, Thus, the model will not be able to perfectly map the distribution. This is particularly important for the larger droplets above about 0.5-1 μm which account for most of the mass carried by the aerosol. The case shown in Figure 11A is for a quite inefficient demister, trying to represent the one installed during the experiments, so the mapping is reasonably good. The integrals under both experimental and model curves, black and green, are the same.

In Figure 12 are shown both experimental and modelled outlet droplet size distributions. The droplet size distribution out was measured both with ELPI+ and with PDI during RUN 4. Also, as for the inlet, the outlet ELPI+ results have been corrected, and both uncorrected and corrected results are shown. We see for the outlet case that the differences between corrected and uncorrected results are visible only for the smallest droplets and that the agreement is much better than for the inlet droplet size distribution. This makes sense as the corrections are mainly for droplet sizes below about 20nm.

Both droplet size distribution instruments used have certain important limitations. The ELPI+ will under-report droplets from about 200-300 nm and above, whereas the PDI only detects droplets from about 400-600nm. It is therefore not unreasonable to assume that the droplet counts in the range 200-1000nm are too low. How low is impossible to know and this picture shows that it is crucial to develop new methods or instruments that are accurate in this range.

The modelled curves are based on the predicted outlet diameters from the demister for the corrected and uncorrected inlet droplet distributions respectively. The corrected curve was adjusted to approximately fit the top of the ELPI+ points. Thus, the absolute values are not
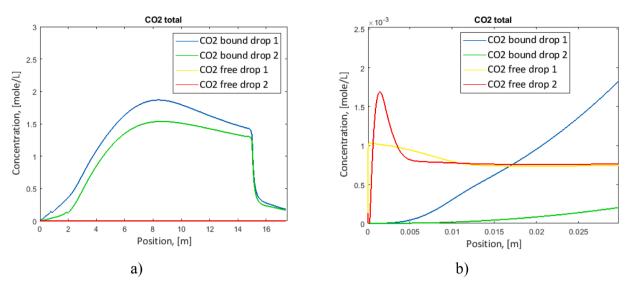
Figure 7. RUN 15 Natural gas exhaust. CO_2 component concentrations as function of position in absorber and water wash, a) full profile, b) magnified inlet section
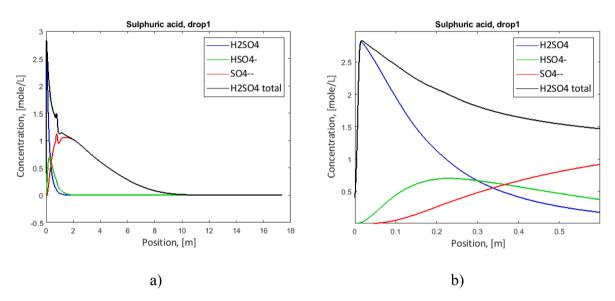

Figure 8. RUN 15 Natural gas exhaust. H_2SO_4 component concentrations in droplet 1 as function of position in absorber and water wash, a) whole column, b) B magnified inlet section

correct. The correct ones are shown in Figure 11. It is not possible to compare a continuous distribution function with measured values for specific size classes, so the modelled curves give an impression of the shape. We see that for the corrected case, the curve under-predicts the experimental results for the droplets up to about 100nm. For larger droplets, in the range above 200nm, the model predicts much higher number concentrations than shown experimentally. The main reason why the model cannot predict the large number of small droplets counted by ELPI+ is that modelling results show that small inlet droplets below about 20nm, hardly grow at all, see later. Thus, the large inlet population of very small droplets pass through the absorber and water wash almost unchanged and contribute to the outlet droplet count. We see this clearly from the corrected outlet counts in Figure 12. The model relies on two parameters, treated as diameters, and with the smallest one well above 20nm, the model will not be able to account for the small droplet classes. On the other hand, these small droplets do not contribute significantly to the overall emissions.

The uncorrected case is normalized such that the integral under the two model curves is the same. For this case, the model is seen to predict a distribution with much larger droplets than the experimental results.

However, with the considerable uncertainty in the experimental results in mind, the model based on the corrected inlet seems to perform reasonably well.

4.6. Single droplet growth

We saw that the model based on a log-normal distribution is able to predict both inlet and outlet size distributions that resemble the experimental ones. However, as mentioned, the model cannot predict the number of tiny droplets passing through the absorber and demister. Therefore, it is of interest to see what the model predicts for droplets so close in size that they can be regarded as a single size. This was done for many droplet sizes and conditions and plotted as seen in Figure 13.

By modelling this outlet size curve formed by the individual points, a relationship between inlet and outlet diameter for single droplets could be obtained for the absorber conditions. We had to choose a droplet number concentration because the number of droplets of a given size will change as they move along the absorber length. We chose 2 droplets/cm³. This choice implies that amine depletion would be negligible in most of the results shown in Figure 13. Possibly, the most exciting
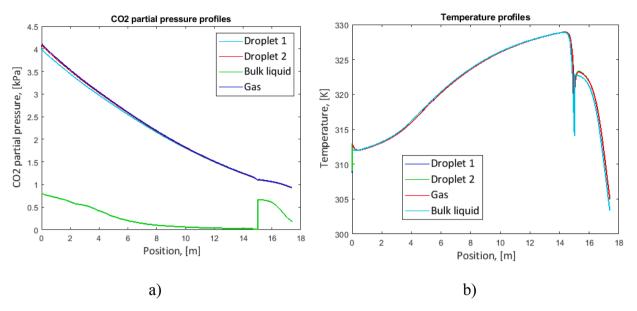
Figure 9. RUN 15 Natural gas exhaust. a): CO_2 partial pressure profile, b): CO_2 partial pressure profile
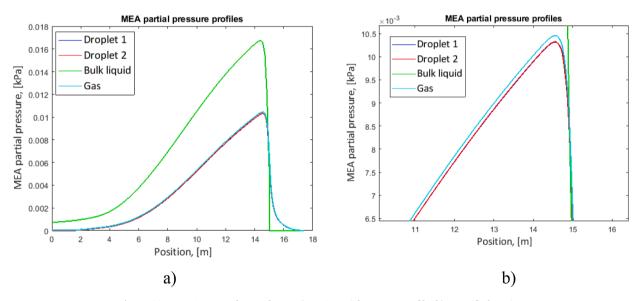

Figure 10. RUN 15 Natural gas exhaust. a) MEA partial pressure profile, b) magnified section

result in Figure 13 is that we see that below about 20nm inlet diameter, the droplets hardly grow at all. For natural gas-based exhaust, the growth is minimal even for droplets up to about 30nm. The Fuchs-Sutugin correction (Fuchs and Sutugin (1971)), the Knudsen effect, for mass transfer to the droplets is used in the model, and for droplets in the range below 20nm it is of the order 0.02-0.1, indicating a strong reduction in mass transfer rate. The Kelvin effect will increase the vapor pressure of the volatile components above small droplets. However, this effect is relatively small and for a droplet of 20nm it increases the vapor pressure of water by about 6%, CO_2 by about 16% and MEA by about 23%. Since the driving forces are small, this is still a significant effect. As indicated earlier, since the two-parameter log-normal model does not have a characterizing droplet size in this range, it will not be able to catch this effect. We also see from Figure 13 that the content of sulphuric acid has a more substantial influence on the growth of the small droplets than for larger ones. This is consistent with earlier findings that the sulphuric acid content does not play a decisive role in the predicted outlet distribution. It is also seen that strong growth prevails almost all the way down to about 20nm for coal-based exhaust and then stops,

whereas, for NG based exhaust, there is a more gradual decrease in growth. This also will influence the comparison between ELPI+ and CPC counts. The CPC counts depend on all droplets growing in the instrument to enable detection. If the smallest droplets do not grow, they will not be counted.

By increasing the inlet droplet number concentration, the effect of gas-phase MEA depletion is seen to have a substantial effect on the growth of the larger droplets, but not for the small ones. This is reasonable as the MEA capacity in the small droplets is low, and their influence is, therefore, also small on MEA depletion.

Finally, the gas superficial velocity is seen to have an effect, reducing the growth with increasing velocity. This is also as expected as the droplets will have less time to grow with high superficial velocities.

4.7. Emissions

In RUN 15, with the demister installed, the total MEA content out was measured with FTIR and found to be 85.4 ppm and in RUN 20, without demister, the result was 87.7 ppm. The accuracy was estimated
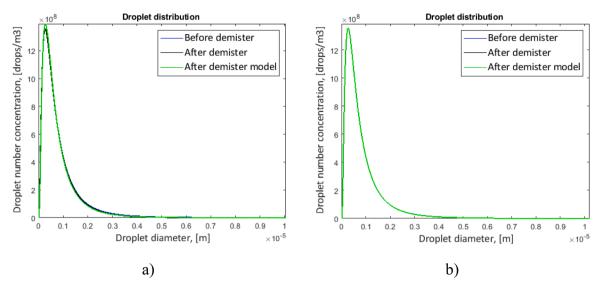
a)

b)

Figure 11. RUN 15 Natural gas exhaust. Droplet size distribution before and after demister: a) With demister, b) Without demister
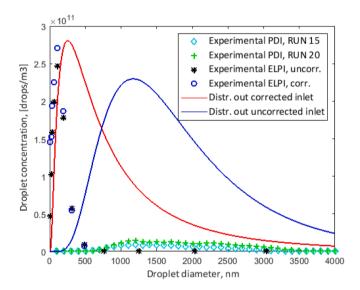

Figure 12. Experimental and modelled outlet droplet size distributions: RUN 15 and RUN 20, Natural gas exhaust.

to ± 5 -10%. The total number of droplets was measured by ELPI+ for RUN 3 and 4 and come in both corrected and uncorrected form. Since RUN 3, 4, 15, and 20 are almost replica of each other, we have assumed that the ELPI+ results are valid for all these four runs.

The emissions predicted by the model depend on the final MEA concentration in the droplets, the droplet size distribution and the total number of droplets. In Table 2 are given predicted emissions from the model under different circumstances compared with available data.

We see that for RUN 20, without demister, the model predicts 99.1ppm using the corrected counts and 90 ppm using the uncorrected ELPI+ counts, both with the corrected inlet distribution. This shows that even if the two predicted outlet distributions, see Figure 12, are quite different, the predicted emissions are relatively close. These numbers are also in the same range as the measured value of 87.7 ppm. In one run, before RUN 20, a Bluefil filter collecting most of the aerosol was installed instead of the normal demister. The liquid collected was analysed for MEA and the amount collected measured. Based on a mass balance, it was estimated that the aerosol in the gas entering the filter contained about 115-125 ppm MEA. The model predicts 230 and 200 ppm entering the demister section with respectively corrected and

uncorrected ELPI+ counts using the corrected inlet distribution and 135 and 117 ppm respectively for uncorrected and corrected counts with the uncorrected inlet distribution. This means that the experimentally found MEA content in the aerosol was reduced from 115-125 to 87.7 ppm in the water wash section. The FTIR measures both gaseous and aerosol MEA from the water wash, but the gaseous part is negligible, i.e. below 1ppm. The model predicts reductions from 230 to 99.1 ppm and from 200 to 90 ppm for the corrected and uncorrected count cases, respectively. It thus may seem that the model overpredicts the reduction in aerosol MEA in the water wash. Possibly some transport properties or reaction rates are over-estimated. As mentioned, the aerosol liquid collected by the filter was analysed and showed a concentration of 3.6-3.9 mol MEA/L. The analyses were done by titration to a pH of about 5 and will not catch MEA bound to sulphuric acid. However, as shown in Figure 8, the sulphuric acid concentrations at the top of the absorber are very low and will not contribute significantly. The model predicts total MEA concentrations of about 5 mol MEA/L, see Figure 6. It should be noted that the model actually predicts the droplet composition at the top of the packing. Above the packing there is about 10 cm headspace, a lean amine inlet distributor, another 40 cm headspace before the demisting section. Above the demisting section, there is about 2m of straight pipe, a 180° bend and then a downflow section leading into the bottom of the water wash section. Both absorber and pipe sections are insulated and placed inside a room at ambient temperature. It is still probable that some condensation takes place in the straight pipe above the demister and that this runs back into the demisting section. This could, at least partly, explain the lower MEA content measured in the demisting section. A low concentration value also affects the estimate of MEA entering the demister.

Experimental results from RUN 15, with demister, can be compared to the model runs with demister in Table 2. We see that using the nominal demister specific area gives predicted MEA emissions of respectively 23.1 and 22.5 ppm for the corrected and uncorrected ELPI+ count cases with the corrected inlet distribution. This can be compared with the experimental value of 85.4 ppm. The demister used was old and, according to the operators, not in good order. Using 50 m²/m³ as specific area, which is very low, we end up with predictions of respectively 72.2 and 64 ppm, still lower than the experimental value. Using the uncorrected inlet distribution, we see that the effect of the demister is weaker, predicting 29 and 25 ppm for the corrected and uncorrected counts, respectively. It is interesting to note that even though the distributions based on corrected and uncorrected inlet size distributions give quite different outlet size distributions, as shown in Figure 12, this
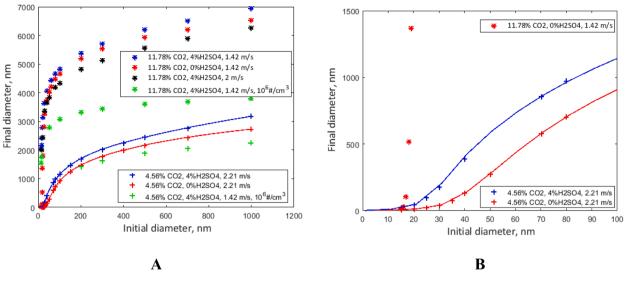
Figure 13. Growth of single droplets in the absorber. **A**: whole range, **B**: Magnified below 100nm

Table 2

Experimental and predicted MEA emissions, Natural gas-based exhaust.

Experimental						
	Run 20 No Demister	*Run 15* With Demister		*Run 20* No Demister	*Run 15* With Demister	
MEA, ppm, out from water wash (FTIR)	85.4	87.7		85.4	87.7	
	Corrected inlet count	Corrected inlet count	Corrected inlet count	Uncorrected inlet count	Uncorrected inlet count	Uncorrected inlet count
Droplets in #/cm³, exp. ELPI+	$1.70 \cdot 10^6$	$1.70 \cdot 10^6$	$1.70 \cdot 10^6$	$1.17 \cdot 10^6$	$1.17 \cdot 10^6$	$1.17 \cdot 10^6$
Droplets out #/cm³, exp. ELPI+	NA	$1.24 \cdot 10^6$	$1.24 \cdot 10^6$	NA	$1.0 \cdot 10^6$	$1.0 \cdot 10^6$
Modeling						
	Run 20 Corrected inlet count	*Run 15* Corrected inlet count	Corrected inlet count	*Run 20* Uncorrected inlet count	*Run 15* Uncorrected inlet count	Uncorrected inlet count
Demister area used in modeling	$0 m^2/m^3$	$50 m^2/m^3$	$360 m^2/m^3$	$0 m^2/m^3$	$50 m^2/m^3$	$360 m^2/m^3$
Droplets out #/cm³, model with corrected inlet distribution	$1.70 \cdot 10^6$	$1.67 \cdot 10^6$	$1.59 \cdot 10^6$	$1.17 \cdot 10^6$	$1.14 \cdot 10^6$	$1.04 \cdot 10^6$
Predicted MEA out, ppm, corrected inlet distribution	99.1	72.2	23.1	90	64	22.5
Droplets out #/cm³, model with uncorrected inlet distribution	$1.70 \cdot 10^6$	$1.65 \cdot 10^6$	$1.46 \cdot 10^6$	$1.17 \cdot 10^6$	$1.126 \cdot 10^6$	$0.96 \cdot 10^6$
Predicted MEA out, ppm, uncorrected inlet distribution	64.9	54.7	29.2	56.5	47.3	24.9

does not give dramatically different predictions for the MEA emissions, see Table 2. For both inlet distributions, significant MEA depletion in the gas is seen. As indicated earlier, in this case the emissions may be mainly determined by the MEA mass transfer from the bulk liquid, which in both cases is very similar.

Also, the number of droplets caught by the demister is calculated by the model. The demister outlet numbers can be compared with the experimental measurements. Using the corrected counts, about 25% of the droplets should have been removed according to the experimental measurements. Since the large droplets are removed with highest efficiency, this measurement seems not to be consistent with the small decrease in MEA emissions when comparing experimental results with and without demister. Using a demister with 50 m²/m³ as specific area, the model predictions indicate only 4-8% removal for both the corrected and uncorrected inlet distribution. Even with these low removal rates, the emissions drop significantly. With the uncorrected counts, the number of droplets removed are close to model predictions using a demister with 360 m²/m³ as a specific area. This indicates both uncertainties in the experimental results and in the efficiency of the demister. The packing itself and the long swan-neck tube section

between demister and water wash may also work as droplet collectors.

In RUN 14, ELPI+ measurements were not available, but CPC counts on the outlet were conducted. These are higher than for the NG- gas case because the gas flow rate is lower, whereas the Topas droplet generator was run under the same conditions as in the NG-gas case, thus providing the same number of droplets. From Table 3 we see that the predicted droplet number concentrations based on the uncorrected inlet number count are more in line with the CPC measurements than those based on the corrected inlet count. The measured outlet emissions of MEA from RUN 14 with the pertinent Topas settings was 193 ppm. The prediction for corrected inlet distribution and with a demister area of 50 m²/m³ are 271 and 219 ppm respectively for the corrected and uncorrected inlet counts, as seen in Table 3. Using the uncorrected inlet distribution, the same predictions are 246.4 and 214 ppm, respectively. The results are slightly higher than the measured value, but they are still considered satisfactory based on uncertainties in both experiments and models. The results for RUN 14 are also consistent with predictions from RUN 15 as they show only moderate differences between corrected and uncorrected inlet droplet size distribution. What may be more surprising is that the model predicts a relatively small difference between using corrected

Table 3

Experimental and predicted MEA emissions, RUN 14, Coal based exhaust

Experimental						
	Run 14 No Demister	With Demister		No Demister	With Demister	
MEA, ppm, out from water wash (FTIR)	–	193		–	193	
	Corrected inlet count	Corrected inlet count	Corrected inlet count	Uncorrected inlet count	Uncorrected inlet count	Uncorrected inlet count
Droplets in #/cm^3, exp	$1.70 \cdot 10^6$	$1.70 \cdot 10^6$	$1.70 \cdot 10^6$	$1.17 \cdot 10^6$	$1.17 \cdot 10^6$	$1.17 \cdot 10^6$
Droplets out #/cm^3, exp. CPC	$1.2 \cdot 10^6$	$1.2 \cdot 10^6$	$1.2 \cdot 10^6$	$1.2 \cdot 10^6$	$1.2 \cdot 10^6$	$1.2 \cdot 10^6$

Modeling						
	Run 14 Corrected inlet count	Corrected inlet count	Corrected inlet count	Uncorrected inlet count	Uncorrected inlet count	Uncorrected inlet count
Demister area used in modeling	0m^2/m^3	50m^2/m^3	360m^2/m^3	0m^2/m^3	50m^2/m^3	360m^2/m^3
Droplets out #/cm^3, model corrected inlet distribution	$1.70 \cdot 10^6$	$1.625 \cdot 10^6$	$1.41 \cdot 10^6$	$1.17 \cdot 10^6$	$1.10 \cdot 10^6$	$0.904\,10^6$
Predicted MEA out, ppm, corrected inlet distribution	405	271.5	87.1	335	218.6	69.1
Droplets out #/cm^3, model uncorrected inlet distribution	$1.70 \cdot 10^6$	$1.617 \cdot 10^6$	$1.363 \cdot 10^6$	$1.17 \cdot 10^6$	$1.101 \cdot 10^6$	$0.903 \cdot 10^6$
Predicted MEA out, ppm, uncorrected inlet distribution	349.6	246.4	88	326	214	68.6

Table 4

The effect of inlet droplet sulphuric acid concentration on emissions*

	Corrected inlet count	Corrected inlet count	Corrected inlet count	Corrected inlet count	Corrected inlet count	Corrected inlet count	Corrected inlet count	Corrected inlet count
Sulphuric acid content, wt %	0 %	1%	4%	8%	0 %	1%	4%	8%
CO2 in inlet gas, vol % dry	4.35	4.35	4.35	4.35	13	13	13	13
Predicted MEA out, ppm	43.9	58.8	64	67.3	214.9	218.9	221.8	233.6

* All data are for corrected inlet distribution, 50 m^2/m^3 demister area and $1.17\,10^6$ droplets/cm^3 in inlet gas.

Table A1

Total pressure P (kPa) and vapour phase mole fraction y of MEA above aqueous mixtures of MEA and Sulphuric acid as function of temperature.

1M H2SO4 + 1M MEA						
T	[°C]	50.54	60.06	69.81	80.65	90.91
P	[kPa]	12.29	19.29	29.79	46.79	69.79
1M H2SO4 + 1.8M MEA						
T	[°C]	50.76	60.27	70.04	80.91	91.16
P	[kPa]	12.28	19.28	29.78	46.78	69.78
1M H2SO4 + 2.4M MEA						
T	[°C]	51.23	60.80	70.56	81.45	91.79
P	[kPa]	12.29	19.29	29.79	46.79	69.78
y	[-]	0.000206527	0.000181	0.000246788	0.000323554	0.000352
2M H2SO4 + 2M MEA						
T	[°C]	52.05	61.6	71.45	82.45	92.76
P	[kPa]	12.29	19.29	29.79	46.79	69.77
2M H2SO4 + 3.8M MEA						
T	[°C]	51.76	64.8	70.44	79.84	90.24
P	[kPa]	11.29	17.78	26.79	39.79	59.78
2M H2SO4 + 4.8M MEA						
T	[°C]	51.22	62.05	71.2	80.26	90.79
P	[kPa]	10.28	16.79	24.78	36.79	55.79
y	[-]	0.001328	0.00122	0.001392	0.001204	0.001194

and uncorrected droplet counts. This is seen both for RUN 15 and RUN 14. This is because a high droplet number concentration leads to higher MEA gas-phase depletion and thus slower droplet growth. The final droplet size distribution is thereby shifted to smaller droplets.

We saw in Figure 4 that the effect of sulphuric acid concentration in the inlet droplets on the outlet droplet size distributions was small and smaller for RUN 14 with coal based exhaust than for RUN 15 with natural gas based exhaust. In Table 4 are shown the predicted MEA emissions as function of sulphuric acid concentration. We see that for

RUN 15 with low CO$_2$ inlet gas concentration, the emissions change going from 0 to 8 wt % sulphuric acid in the inlet droplets is about 50%, whereas for RUN 14 it is less than 10%. The difference between RUN 14 and RUN 15 is in line with what was seen in Figure 4. However, the apparently small variations seen in the size distributions in Figure 4 for RUN 15 do result in significant differences in actual emissions. It should be noted that in the simulations performed in this work, the droplet number and sulphuric acid concentrations were predetermined. Therefore, the results may not be directly applicable for cases where SO$_3$
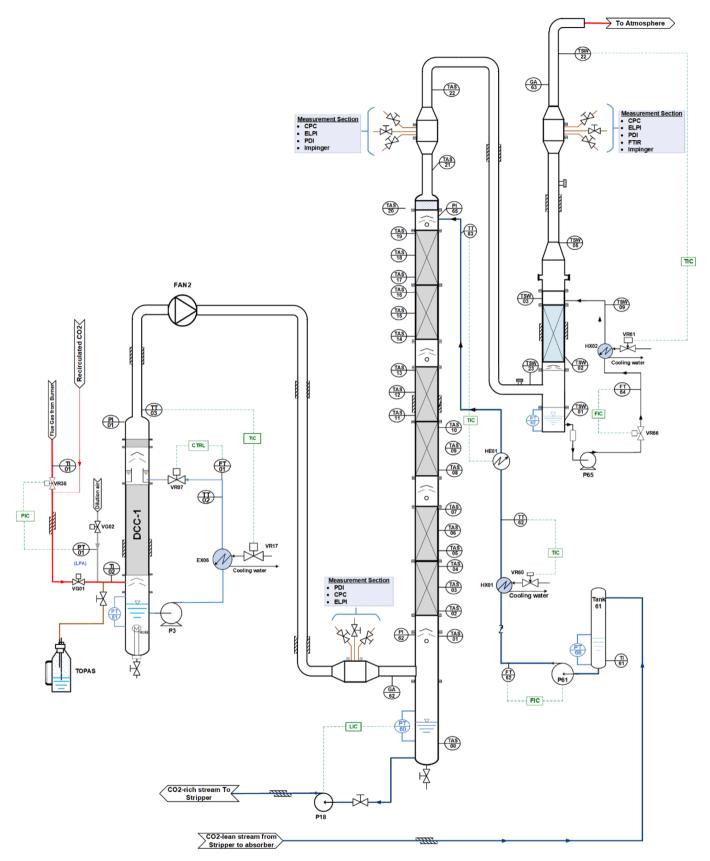
Figure A1. Absorber and water wash system used in the Aerosolv experiments showing the Topas droplet generator, direct contact cooler, measurement sections and layout of gas flow path.

enters with the inlet gas causing condensation and sulphuric acid formation on nuclei in the gas.

In the Supplementary information are given MEA concentration profiles, MEA partial pressure profiles and the droplet size profiles for 0, 1, 4 and 8 wt% H_2SO_4 in the initial droplets. In Figure S3 we see that the initial drop in size is very large for the sulphate-free droplets and gradually decreases as the sulphate content increases. The final drop size goes down with increasing sulphate content for droplet 1 and up for droplet 2. This means that the size distribution widens. In Figure S2 are given the MEA partial pressure profiles. At zero sulphate content, the MEA partial pressure almost immediately increases and approaches the bulk liquid MEA pressure. As the sulphate content increases it takes longer and longer before the MEA partial pressure becomes significant. This implies that the overall driving force for MEA between bulk fluid and droplets increases with increasing sulphate content. As discussed earlier, the MEA mass transfer from the bulk liquid largely determines the emissions, and the increase in driving force can thus explain the seen increase in emissions with sulphate content. In Figure S1 the MEA concentration profiles are given for droplet 1. The trend is similar for droplet 2. Without sulphate the MEA content increases rapidly, explaining the rapid increase in MEA partial pressure seen in Figure S2. However, the final total MEA concentration after the water wash can be seen to increase with increasing sulphate content. In conclusion, increased sulphate content increases the final MEA concentration, increases overall MEA driving forces and widens the droplet size distribution.

Based on the results shown, it is difficult to decide whether to rely on the uncorrected or corrected inlet droplet distribution. The corrected inlet distribution is seen to give an outlet distribution curve more in line with the measured outlet distribution. However, the impact on the actual emissions predictions is not dramatic. As mentioned, this is probably because the total emission is largely determined by the mass transfer rate from the bulk liquid. We are satisfied that the predicted emissions are in the right order of magnitude and only a factor of about 1-3 from the reported experimental values.

When using the experimental droplet counts for the various size classes from the outlet ELPI+ and PDI measurements together with the model predicted outlet MEA concentration in the droplets, the total emissions based on ELPI+ was found to be negligible because of the small sizes. Similarly, the total based on the PDI measurements was found to account for about 20 ppm, or about 25% of the measured emissions value. This shows that there is a large amount unaccounted for.

It should be noted that the predicted gas-phase emission of MEA is in the order >1 ppm, and thus insignificant.

5. Conclusions

A new and improved aerosol model has been developed and tested against experimental data obtained at the Tiller CO_2 capture facility in Norway.

An earlier e-NRTL equilibrium model for MEA was extended to cover sulphuric acid containing droplets and implemented in the aerosol model. The model was adjusted for water and MEA volatility based on new ebulliometer experiments on the unloaded MEA/water/H_2SO_4 system. Comparisons between experimental and calculated partial pressures show good agreement for water and reasonable agreement for MEA.

Experimental droplet input distributions based on ELPI+ measurements were fitted to a log-normal distribution model and, together with number concentrations from ELPI+ and CPC, used as model input.

The model predicted outlet droplet distributions were compared with outlet ELPI+ and PDI measurements. The model outlet droplet distribution covered the whole range of ELPI+ and PDI sizes and predicted higher number concentrations in the intermediate size range between 200 and 800 nm where both the experimental techniques

counted very few droplets. The experimental counts from both techniques were integrated using the model droplet MEA concentration and compared with emissions measured with FTIR. ELPI+ was found to account for a negligible amount of the emissions and PDI for about 25% of the emissions.

The droplet model predicts emissions without demister installed in the absorber, within $\pm$ 20% of the experimental value. With demister, the results depend largely on the demister efficiency and the model predicts 30-80% of the measured emissions dependent on efficiencies used. The model predicts very well the change in emissions when shifting from NG-based to coal-based exhaust.

Under conditions reported in this work, the droplet number concentration was found to have only a small effect on the predicted emissions. We see more MEA gas-phase depletion with high droplet concentrations and thus slower growth. The effects of higher number concentration and smaller size counteract each other. We also see that in the case of significant MEA depletion in the gas phase, the emissions are largely determined by the mass transfer rate from the bulk liquid.

The initial droplet sulphuric acid concentration was found to have only a small effect on the outlet droplet size distribution. However, the effect on MEA emissions was significant: the emissions went up as the initial sulphuric acid concentration increased even though the final concentration in the outlet droplets was almost negligible. The effect of sulphuric acid was much stronger for low inlet gas CO_2 content (NG) than for coal-based exhaust. The increase in emissions is believed to be caused by an increase in the overall driving force for MEA between bulk liquid phase and droplet when sulphuric acid is present.

The log-normal model size distribution is seen not to catch the tiny inlet droplet sizes in the range below 20-30nm. Modeling using single size droplets show that these droplet sizes hardly grow in the absorber and water wash but pass straight through. In the total emissions, these droplets, although in large number concentrations, have a negligible impact on the emissions.

To validate the droplet model further, experimental data for droplet size distributions covering the whole size range with good accuracy are needed. Also, a more accurate model for the demister is necessary.

Author contributions

Hallvard F. Svendsen: Model development, conceptualization, writing original draft and review

Hammad Majeed: Earlier model development

Hanna Knuutila: Project administration, resources

Magne Hillestad: Conceptualization

Sigvart Evjen: Experimental work laboratory

Thor Mejdell: Experimental work pilot plant

Kai W. Hjarbo: Experimental work pilot plant

Geir Haugen: Simulation software

Karl A. Hoff: Project administration pilot work

Aslak Einbu: Project administration pilot work

Declaration of Competing Interest

The authors declare no competing financial or other conflict of interest.

Acknowledgments

The ELPI+ droplet size measurements were performed by ENGIE Laborelec, Simon Boulivardlaan 34,1000 Brussels, Belgium.

Supplementary materials

Supplementary material associated with this article can be found, in the online version, at doi:10.1016/j.ijggc.2021.103390.

Appendix

Table A1, Figure A1.

References

AMACS, 2004. The Engineered Mist Eliminator [WWW Document]. https://www.amacs.com/. URL https://www.amacs.com/wp-content/uploads/2012/09/AMACS-Mist-Eliminator-Brochure6.pdf , (accessed 2020.12.03).

Anonymous, 2005. The engineered mist eliminator. Chemical Engineering Progress 101 (6), 1–13.

Ashgriz, N., 2011. Handbook of Atomization and Sprays: Theory and Applications. Springer Science & Business Media. ISBN 978-1-4419-7264-4.

Bachalo, W.D., 1980. Method for Measuring the Size and Velocity of Spheres by Dual-beam Light Scatter Interferometry. Applied Optics 19 (3), 363–370. https://doi.org/10.1364/AO.19.000363.

Bade, O.M., Knudsen, J.N., Gorset, O., Askestad, I., 2014. Controlling amine mist formation in CO_2 capture from residual catalytic cracker (RCC) flue gas. Energy Proc 63, 884–892. https://doi.org/10.1016/j.egypro.2014.11.098.

Beaudry M., Fulk S., Rochelle G.T., Field measurements of amine aerosol by FTIR and phase Doppler interferometry, 114 (2017) 906-929, https://doi.org/10.1016/j.egypro.2017.03.1234.

Biesenberger, J.A., Sebastian, D.H., 1983. Principles of polymerization engineering. Wiley Interscience.

Brachert, L., Mertens, J., Khakharia, P., Schaber, K., 2014. The challenge of measuring sulfuric acid aerosols: number concentration and size evaluation using a condensation particle counter (CPC) and an electrical low-pressure impactor (ELPI +). J. Aerosol Sci. 67 https://doi.org/10.1016/j.jaerosci.2013.09.006.

Bürkholz, A., 1989. Droplet separation. VCH Publishers, New York.

Carter T., National Carbon capture CenterPost-combustion, 2012 NETL CO2 Capture Technology Meet (2012), https://netl.doe.gov/node/8424#tue2 , (accessed 2020.12.03).

Da Silva, E.F., Kolderup, H., Goetheer, E., Hjarbo, K.W., Huizinga, A., Khakharia, P., Tuinman, I., Mejdell, T., Zahlsen, K., Vernstad, K., Hyldbakk, A, Holten, T, Kvamsdal, H.M., van Os, P., Einbu, A., 2013. Emission studies from a CO_2 capture pilot plant. Energy Proc 37, 778–783. https://doi.org/10.1016/j.egypro.2013.05.167.

Davis, E.J., 1982. Transport phenomena with single aerosol particles. Aerosol Sci. Technol. 2, 121–144. https://doi.org/10.1080/02786828308958618.

Einbu, A., 2016. CO2SIM (Flowsheet Simulator for CO2 Absorption Processes) [WWW Document]. SINTEF. URL https://www.sintef.no/en/software/co2sim-flowsheet-simulator-for-co2-absorption-proc/ (accessed 2020.11.23).

Fuchs, N.A., Sutugin, A.G., 1971. In: Hidy, G.M., Brock, J.R. (Eds.), Topics in current aerosol research. Oxford, 2. Pergamon Press, pp. 1–60. https://doi.org/10.1016/C2013-0-02462-0.

Fulk, S., Rochelle, G.T., 2013. Modeling aerosols in amine-based CO_2 Capture. Energy Proc 37, 1706–1719. https://doi.org/10.1016/j.egypro.2013.06.046.

Fulk, S., Rochelle, G.T., 2014. Quantification of gas and aerosol-phase emissions by FTIR under variable bench-scale absorber conditions. Energy Proc 63, 871–883. https://doi.org/10.1016/j.egypro.2014.11.097.

Fulk, S., Beaudry, M.R., Rochelle, G.T., 2017. Amine Aerosol characterization by Phase Doppler Interferometry. Energy Proc 114, 939–951. https://doi.org/10.1016/j.egypro.2017.03.1237.

Fujita, K., Muraoka, D., Kaseda, T., Saito, S., Kitamura, H., Kato, Y., Udatsu, M., Handa, Y., Suzuki, K., 2017. Impact of the Aerosol Particle Included in Actual Flue Gas on Amine Mist Formation/Growth in the Post-Combustion Capture Pilot Plant. Energy Procedia 114, 930–938. https://doi.org/10.1016/j.egypro.2017.03.1235.

Hartono, A., Saleem, F., Arshad, M.W., Usman, M., Svendsen, H.F., 2013. Binary and ternary VLE of the 2-(Diethylamino)ethanol(DEEA) /3-(methylamino) propylamine (MAPA) / water system. Chem Eng. Science 101, 401–411. https://doi.org/10.1016/j.ces.2013.06.052.

Hartono, A., Mba, E.O., Svendsen, H.F., 2014. Physical properties of partially loaded aqueous monoethanolamine(MEA). J. Chem. Eng. Data 59, 1808–1816. https://doi.org/10.1021/je401081e.

Johnson, N.L., Kotz, S., Balakrishnan, N., 1994. Continuous Univariate Distributions, edition. ed., 1, 2. Wiley-Interscience, New York. ISBN: 978-0-471-58495-7.

Kamijo, T., Kajiya, Y., Endo, T., Nagayasu, H., Tanaka, H., Hirata, T., Yonekawa, T., Tsujiuchi, T., 2013. SO3impact on amine emission and emission reduction technology. Energy Procedia 37, 1793–1796. https://doi.org/10.1016/j.egypro.2013.06.056.

Kang, J.-L., Zhang, Y., Fulk, S., Rochelle, G.T., 2017. Modeling amine aerosol growth inthe absorber and water wash. Energy Procedia 114, 959–976. https://doi.org/10.1016/j.egypro.2017.03.1241.

Kang, J.-L., Liu, K-T., Wong, D.S-H., Jang, S-S., Tsai, D-H., 2020. Multi-scale modeling and study of aerosol growth in an amine-based CO_2 capture plant. Environments 7, 58. https://doi.org/10.3390/environments7080058.

Khakharia, P., Brachert, L., Mertens, J., Huizinga, A., Schallert, B., Schaber, K., Vlugt, T.J.H., Goetheer, E., 2013. Investigation of aerosol based emission of MEA due to sulphuric acid aerosol and soot in a Post Combustion CO_2 Capture process. Int. J. Greenh. Gas Control. 19, 138–144. https://doi.org/10.1016/j.ijggc.2013.08.014.

Khakharia, P., Mertens, J., Vlugt, T.J.H., Goetheer, E., 2014. Predicting aerosol emissions in a post combustion CO_2 capture process using and Aspen Plus model. Int. J. Greenh. Gas Control. 63, 911–925. https://doi.org/10.1016/j.ijggc.2014.11.101.

Khakharia, P., Brachert, L., Mertens, J., Anderlohr, C., Huizinga, A., Fernandez, E.S., Schallert, B., Schaber, K., Vlugt, T.J.H., Goetheer, E., 2015. Understanding aerosol-based emissions in a post combustion CO_2 capture process: parameter testing and mechanisms. Int. J. Greenh. Gas Control. 34, 63–74. https://doi.org/10.1016/j.ijggc.2015.01.001.

Khakharia, P., Mertens, J., Abu-Zahra, M.R.M., Vlugt, T.J.H., Goetheer, E.L.V., 2016. Overview of aerosols in post-combustion CO2capture. Absorption-Based Post-Combustion Capture of Carbon Dioxide. Elsevier 465–485. https://doi.org/10.1016/B978-0-08-100514-9.00019-6.

Knudsen, J.N., Andersen, J., Jensen, J.N., Biede, O., 2011. Evaluation of process upgrades and novel solvents for the post combustion CO_2 capture process in pilot-scale. Energy Procedia 4, 1558–1565. https://doi.org/10.1016/j.egypro.2011.02.025.

Kim, I., Svendsen, H.F., Børresen, E., 2008. Ebulliometric Determination of Vapor−Liquid Equilibria for Pure Water, Monoethanolamine, N-Methyldiethanolamine, 3-(Methylamino)-propylamine, and Their Binary and Ternary Solutions. Journal of Chemical & Engineering Data 53, 2521–2531. https://doi.org/10.1021/je800290k.

Lombardo, G., Fostås, B.F., Shah, M.I., Morken, A.K., Hvidsten, O.A., Mertens, J., Hamborg, E.S., 2017. Results from aerosol measurement in amine plant treating gas turbine and Residue Fluidized Catalytic Cracker flue gases at the CO_2 Technology Center Mongstad. Energy Proc 114, 210–230. https://doi.org/10.1016/j.egypro.2017.03.1377.

Majeed, H., Knuutila, H., Hillestad, M., Svendsen, H.F., 2017a. Gas phase amine depletion created by aerosol formation and growth. Int. J. Greenh. Gas Control 64, 212–222. https://doi.org/10.1016/j.ijggc.2017.07.001.

Majeed, H., Knuutila, H.K., Hillestad, M., Svendsen, H.F., 2017b. Characterization and modelling of aerosol droplet in absorption columns. Int. J. Greenh. Gas Control 58, 114–126. https://doi.org/10.1016/j.ijggc.2017.01.006.

Majeed, H., Svendsen, H.F., 2018a. Characterization of Aerosol Emissions from CO2 Capture Plants treating various Power Plant and Industrial Flue Gases. Int. J. Greenh. Gas Control 74, 282–295. https://doi.org/10.1016/j.ijggc.2018.04.016.

Majeed, H., Svendsen, H.F., 2018b. Effect of Water Wash on Mist and Aerosol Formation in Absorption Column. Chem. Eng. J 333 (2018), 636–648. https://doi.org/10.1016/j.cej.2017.09.124.

Majeed, H., Knuutila, H.K., Hillestad, M., Svendsen, H.F., 2018c. Predicting aerosol size distribution development in absorption columns. Chemical Engineering Science 192 (2018), 25–33. https://doi.org/10.1016/j.ces.2018.07.004.

T. Mejdell, Einbu A., Hoff K.A., Hjarbo K., Rogiers P., Lepaumier H., Svendsen H.F., Aerosols characterization and emission control at Tiller plant 15th International Conference on Greenhouse Gas Control Technologies GHGT-15 15th-18th March 2021; https://ssrn.com/abstract=3819334.

Mertens, J., Knudsen, J., Thielens, M-L., Andersen, J., 2012. On-line monitoring and controlling emissions in amine post combustion carbon capture: A field test. Int. J. Greenh. Gas Control. 6, 2–11. https://doi.org/10.1016/j.ijggc.2011.11.015.

Mertens, J., Brachert, L., Desagher, D., Thielens, M.L., Khakharia, P., Goetheer, E., Schaber, K., 2014. ELPI+ measurements of aerosol growth in an amine absorption column. Int. J. Greenh. Gas Control. 23 (2014a), 44–50. https://doi.org/10.1016/j.ijggc.2014.02.002.

Mertens, J., Lepaumier, H., Desagher, D., Thielens, M.-L., 2013. Understanding ethanolamine (MEA) and ammonia emissions from amine based post combustion carbon capture: lessons learned from field tests. Int. J. Greenh. Gas Control. 13, 72–77. https://doi.org/10.1016/j.ijggc.2012.12.013.

Mertens, J., Brachert, L., Desagher, D., Schallert, B., Khakharia, P., Goetheer, E., 2014b. Predicting amine mist formation based on aerosol number concentration and size measurements in flue gas. Energy Procedia 63, 893. https://doi.org/10.1016/j.egypro.2014.11.099.

Perry, R.H., Green, D.W., 2007. Perry's Chemical Engineers' Handbook, 8th edition. McGraw Hill, NY.

Putta, K.R., Pinto, D.D.D., Knuutila, H.K., Svendsen, H.F., 2016. CO_2 absorption into loaded MEA solutions: Kinetics assessment using penetration theory. International Journal of Greenhouse Gas Control 53, 335–353. https://doi.org/10.1016/j.ijggc.2016.08.009.

Qu, X., Davis, E.J., 2001. Droplet evaporation and condensation in the near-continuum regime. Aerosol Science 32 (2001), 861–875. https://doi.org/10.1016/S0021-8502(00)00112-9.

Saha, C., Irvin, J.H., 2017. Real-time aerosol measurements in pilot scale coal fired post-combustion CO_2 capture. J. Aerosol Sci. 104, 43. https://doi.org/10.1016/j.jaerosci.2016.11.005.

Snijder, E.D., te Riele, M.J.M, Versteeg, G.F., Van Swaaij, W.P.M., 1993. Diffusion coefficients of several aqueous alkanolamine solutions. Journal of Chemical and Engineering Data 38 (3), 475–480. https://doi.org/10.1021/je00011a037.

Trollebø, A.A., Hartono, A., Usman, M., Saeed, M., Svendsen, H.F., 2020. Vapour-liquid equilibria in pure N-Methyl-1,3-diaminopropane (MAPA), 1,3-diaminopropane (DAP), 2-(Isopropylamino)ethanol (IPAE), N-tert-Butyldiethanolamine (N-TBDEA)

and their aqueous solutions. Journal of Chemical Thermodynamics 141, 105965. https://doi.org/10.1016/j.jct.2019.105965.

Zhang, Y., Kang, J.-L., Fulk, S., Rochelle, G.T., 2017. Modeling amine aerosol growth at realistic pilot plant conditions. Energy Procedia 114, 959–976. https://doi.org/10.1016/j.egypro.2017.03.1251.